Nøyaktighetsundersøkelse av fotogrammetrisk kartlegging med drone i et testfelt i Norge

Hossein Nahavandchi[1], Trond Arve Haakonsen[1] and Håvard Aas[2]

Hossein Nahavandchi et al.: Accuracy investigations of UAV Photomapping over a test area in Norway

KART OG PLAN, Vol. 76, pp. 250–264, POB 5003, NO-1432 Ås, ISSN 0047-3278

Drone systems are high-technology products which can also be used for mapping. Drone mapping has recently become very popular for producing orthophoto maps, terrain models and 3D-data over small areas. A test area located at the Norwegian University of Science and Technology, Trondheim was used. To investigate the accuracy of drone mapping systems, we produced a 3D photogrammetric model of the test area. 18 ground control points were created and measured by the Global Navigation Satellite System (GNSS). The model was then georeferenced and fitted to 8 ground control points. We then examined the accuracy of the drone map using control points not used in georeferencing process. The root mean square errors in horizontal and vertical positions were estimated at 3.2 cm and 6.8 cm respectively.

Key words: digital surface model, drone, georeferencing, ground control point, orthophoto

Hossein Nahavandchi, Norwegian University of Science and Technology, Division of Geomatics, NO-7491 Trondheim. E-mail: hossein.nahavandchi@ntnu.no

1. Introduction

From property management to construction, from forestry to real estate, everybody uses maps. There are so many uses for up-to-date high quality maps that it would be impossible to list them all. Unmanned Aerial Systems (UAS) are known under various names and acronyms, such as Unmanned Aerial Vehicle (UAV), Remotely Piloted Aircraft System (RPAS), Aerial Robot, or simply «Drone». The components of a Drone mapping system are an unmanned aircraft (in this study), a ground control and a communication system.

The development of UAVs started in the 1950's for military purposes. The aim was to produce vehicles capable of carrying missions with no onboard pilot. However, other applications of UAVs, for example aerial photography for survey purposes, have become a focus of attention for civil society (see, e.g., Mills and Newton 1996; Mills et al. 1996).The market for UAVs is growing rapidly. The success in the military field has provided a platform and stimulus for development of multi-sensor platforms for civil applications.

Manufacturing companies have offered multi-sensor platforms for several years. In addition to other features, they are equipped with an integrated navigation unit consisting of Global Navigation Satellite System (GNSS) receivers, an Inertial Measurement Unit (IMU), and an optical 3D measurement system mostly composed of one or several laser scanners and cameras. Such systems have, however, been expensive with an estimated price of starting at US$120000. The sensors can be adapted to planes, helicopters or land crafts.

Use of UAV systems in photogrammetric applications is expanding rapidly. Several research groups have studied the capability of UAVs in production of digital maps (see, e.g., Eisenbeiß 2009; Ahmad 2011; Harwin and Lucieer 2012; Rosnell and Honkavaara 2012; Mancini et al. 2013). The technological devel-

1. Division of Geomatics, Department of Civil and Environmental Engineering, Norwegian University of Science and Technology
2. Blinken Nord As

opment of navigation systems allows reduced cost and miniaturization of payloads. Projects can now be set up based on «low-cost» platforms. Small areas, especially, are suitable for 3D data acquisition using low-cost UAVs that are both cost effective and flexible.

UAVs can be flown by electronic equipment on the vehicle and at a Ground Control Station (GCS), or directly from the ground. In the latter case the system is commonly called RPV (Remotely Piloted Vehicle), since the vehicle is remotely piloted and operated by radio-controlled devices.

The objective of this study is to investigate the capability of a UAV in producing digital photomaps and to assess the accuracy of mapping using UAV technology. Ground control points established and measured by GNSS are used for accuracy analysis.

2. The UAV project

The Norwegian Road and Transport Administration (SVV) is preparing to map roads using UAVs. In this study we carry out an operational UAV mapping for analysis and evaluation of how Drone data can support the work of the SVV. To this purpose, the Norwegian University of Science and Technology (NTNU), division of Geomatics, in cooperation with Blinken AS, has tested a «low cost» (compared to the classical photogrammetry) mini-UAV called «eBee». eBee is a remote controlled aircraft equipped with a GPS/IMU navigation system and a standard 16 MB RGB camera as a photographic sensor. The camera is suitable for digital photogrammetric shootings with satisfactory geometric and radiometric quality.

2.1 The UAV «eBee»

The UAV eBee (the professional mapping drone) is developed and patented by «senseFly,» a Parrot company which designs, assembles and market autonomous mini-drones and related software solutions for civil professional applications. These include precision agriculture, land surveying, GIS, construction and environmental conservation. In addition to eBee, «senseFly» has made four other drones: «eXom» (the inspection and close mapping drone); «eBee RTK» (the survey-grade mapping drone); «eBee Ag» (the precision agriculture drone); and «swinglet CAM» (the professional GIS drone). Our attention turned to the eBee (the professional mapping drone) due to the availability of this model in Blinken AS, our partner in the UAV test analysis. The UAV eBee (the professional mapping drone) is shown in Figure 1. The eBee hardware is characterized by a conventional configuration: fixed wing with a wingspan 96 cm and approximate weight of 0.69 kg, tailless integrated wing-fuselage, and tractor propeller

Figure 1. The UAV eBee (the professional mapping drone)

driven with a 160W brushless DC motor. The material is EPP foam, carbon structure and composite parts. The battery is rechargeable Lithium-Polymer 11.1 V, 2150 mAh. The fixed-wing configuration gives the eBee a better capability of withstanding adverse weather conditions, such as gusts, and also allows larger payload capabilities and produces superior flight performance.

2.2. Navigation system

The eBee is equipped with onboard artificial intelligence that allows autonomous flights and provides a real-time attitude of flight. The artificial intelligence inside the eBee's autopilot continuously analyses data provided by the IMU and onboard GPS to control every aspect of its flight. The system also includes ground station control software (eMotion). Using eMotion software one can view the eBee's flight parameters, battery level and image acquisition progress in real time. The artificial intelligence inside the eBee's autopilot communicates with the ground station software eMotion via a 2.4 GHz radio link with the USB ground modem.

The software eMotion is used to plan and simulate a mapping mission. eMotion provides flight path and current sensor values in real time. The operator can also insert a flight plan onto a preloaded (base) map and upload these during the flight. In the base map one can define the area to be covered by the eBee. The required ground resolution can be specified with a Ground Sampling Distance (GSD) down to 1.5 cm, and image overlap. eMotion automatically generates a full flight plan, calculates the eBee's required altitude and displays its projected trajectory. If the flying area includes uneven terrain, the eMotion's 3D mission planning feature takes the elevation data into account when setting the altitude of waypoints and the resulting flight lines. This improves ground resolution and increases safety. To ensure mission success, eMotion runs a virtual flight that simulates wind strength and direction. Then it makes any flight plan updates required and prepares to launch. The system can also be connected to the payload cameras, so it is possible to schedule an automatic shooting time. Optimum range limit is up to 50 min flight time for coverage of up to 12 km^2. The take-off operation is manual and landing is usually made according to the flight plan. The linear landing accuracy is approximately 5 m.

2.3. Sensors

The current configuration of the UAV allows onboard digital sensors for video and imagery acquisition to be carried. The eBee is equipped, as standard, with a Canon 16 MB RGB IXUS/ELPH camera. Two additional cameras are also available, which may always be used one at a time. The camera system also includes a 16 GB SD card, battery, USB cable and charger. The approximate take-off weight of the eBee, including camera, is 0.69 kg. The camera is controlled by eBee's autopilot and it captures images automatically. The motors are turned off during imaging to avoid vibration. The images taken by the camera can be transformed into 2D orthomosaics and 3D models with absolute horizontal/vertical accuracy as high as 3 cm/5 cm.

3. Flight planning and aerial survey

3.1 Flight Planning

In order to generate 3D information from aerial photographs a flight plan has to be made. A flight planning tool capable of flight plan simulation has been developed for eBee. senseFly's intuitive eMotion software is used to plan and simulate the mapping mission. After selecting the area of interest, for example in Google Earth, one can import the base map and then specify the required ground resolution and image overlap. The GSD can be selected down to 1.5 cm. eMotion then automatically generates a full flight plan, calculating the eBee's required altitude and displaying its projected trajectory. If one is planning to fly the eBee in extreme situations, such as mountainous area with uneven terrain, one can use eMotion's 3D mission planning feature to take elevation data into account when setting the altitude of waypoints and the resulting flight lines. This improves ground resolution and increases safety.

3.2 Aerial Survey

After setting up the aerial survey the eBee is ready for launch. There are no flying skills

required. By shaking eBee three times it starts its motor, and then we just throw it into the air. The artificial intelligence system inside the eBee's autopilot continuously analyses data provided by the IMU unit and onboard GPS to control every aspect of its flight. Using eMotion ground station software, one can view the eBee's flight parameters, battery level and image acquisition progress in real time. It is possible to re-program the eBee's flight plan mid-flight if any mistake is made during planning, and even land the eBee mid-flight.

The advanced software package, eMotion, configures the camera to capture multiple images. The interval between images is about 2 seconds so that at least two pictures will be captured at every waypoint. After reaching the predefined altitude, the flight direction is controlled and corrected if necessary. The eBee is then set to GPS waypoint mode in order to head for the first loaded waypoints. Tests have shown that flying the eBee in 6-8 m/s breezes is feasible without a problem. Wind speeds above ca. 12 m/s led to distinct differences from preset waypoint coordinates. After having successfully flown to all waypoints, the landing function is activated and landing can be prepared. This is the final step in the data acquisition.

3.3 Post-processing Software

The eBee is supplied with an advanced software package for post-processing the data. It is named Postflight Terra 3D (professional photogrammetry). This software processes the flight's photos. The software uses bundle adjustment for image processing.

The common post-processing software for the UAV automatically generates geo-referenced 2D orthomosaic, 3D point clouds, triangle models, Digital Elevation Models or Digital Surface Models (DSMs) from arbitrary image configurations. A more detailed procedure to generate photogrammetric products such as DSMs can be found in Eisenbeiß (2009). Interior and exterior orientation are computed in a bundle adjustment by automatically extracting features such as contours, edges, and feature points (key points or tie points), which then have to be allocated in order to describe homologous areas. In a bundle adjustment with at least 60 % longitudinal overlap and 20 % lateral coverage, one computes the relations between images coordinates and object coordinates directly. In this case, the image is the elementary unit in a bundle adjustment with no introduction of model coordinates as an intermediate step (see, e.g., Kraus 2011). The data used in the bundle adjustment consist of the image coordinates of the tie points, plus the image coordinates and object coordinates of the ground control points. Tie points are the points existing in more than one image. The image coordinates and the associated projection center of an image define a spatial bundle of rays that for a set of images is called bundle adjustment. Figure 2 (Kraus 2011) shows camera projection centers and planes in negative positions in the 3D terrain coordinate system. Ground control points with known *xyz*-coordinates in the terrain system are shown with a circle inside a triangle. Black-filled circles symbolize so-called tie points. The tie point coordinates in the terrain system are not known. One straight line (or one single ray from a bundle), in Figure 2, geometrically represents the mathematical relation between a point in the image plane, through its respective projection center to the corresponding object point in the terrain. The elements of exterior orientation of all bundles in the images are computed simultaneously. The adjustment principle is to displace and rotate the bundle of rays so that the bundles intersect each other at the tie points and pass through the control points in a least-squares sense. This means that in a central projection, the image point, the projection center and the object point should be in a straight line (the collinear condition). Because of small random observation errors they are not, so corrections $v_{\bar{\xi}_{ij}}$ and $v_{\eta_{ij}}$ are introduced to the pairwise measured image coordinates $(\bar{\xi}_{ij}, \bar{\eta}_{ij})$ in order to solve for unknown parameters iteratively in a least-squares sense. Each measured image point yields two observation equations (see, e.g., Kraus 2011):

$$
\begin{aligned}
v_{\xi_{ij}} &= \left(\frac{\partial \xi}{\partial X_{0j}}\right)^0 dX_{0j} + \left(\frac{\partial \xi}{\partial Y_{0j}}\right)^0 dY_{0j} + \left(\frac{\partial \xi}{\partial Z_{0j}}\right)^0 dZ_{0j} \\
&+ \left(\frac{\partial \xi}{\partial \omega_{0j}}\right)^0 d\omega_{0j} + \left(\frac{\partial \xi}{\partial \varphi_{0j}}\right)^0 d\varphi_{0j} + \left(\frac{\partial \xi}{\partial \kappa_{0j}}\right)^0 d\kappa_{0j} \\
&+ \left(\frac{\partial \xi}{\partial X_i}\right)^0 dX_i + \left(\frac{\partial \xi}{\partial Y_i}\right)^0 dY_i + \left(\frac{\partial \xi}{\partial Z_i}\right)^0 dZ_i \\
&- \left(\bar{\xi}_{ij} - \xi_{ij}^0\right)
\end{aligned}
\tag{1}
$$

The expression for $v_{\eta_{ij}}$ has a similar form. The unknowns are the six exterior orientation parameters of the camera projection center positions (X_0, Y_0, Z_0) and its three rotations (ω, φ, κ) of the photograph with the index *j,* and ground point coordinates (X_i, Y_i, Z_i) for any tie point number *i*. The superscript zero indicates that the coefficients are computed from approximate values. During this adjustment, calibration parameters of the camera can also be estimated. It should be mentioned here that a preliminary computation is made to estimate from the navigation system the approximate values of exterior orientation parameters. A final least-squares adjustment is then made using ground control and tie points. We call this process georeferencing. There are reasons to believe that the Postflight Terra 3D software uses a more advanced least-squares model, handling the six external parameters as stochastic rather than fixed parameters, but to date this model is a trade secret.

3.4 Georeferencing

Several ground control points located within the area of interest are used in the georeferencing process. These points were signalized with 15 cm colored targets and then surveyed by GNSS receivers. After the aerial survey carried out the targets had to be detected within the images.

The coordinates of ground control points have been computed based on the observation techniques for classic static GNSS baselines. Baseline components in an Earth fixed Carte-

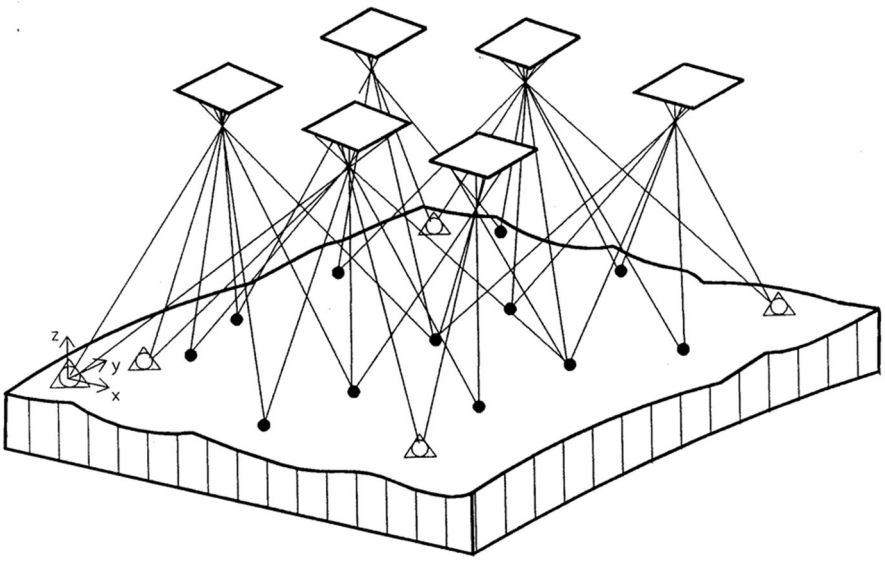

Figure 2. Principle of a bundle adjustment

sian system and their covariance matrices have been processed in the Leica LGO v8.2 software, and then exported to be used as observations in the GISLine v5.3 software. Each baseline has been converted to triplets of: slope distance, geodetic azimuth and zenith angle, which are the basis observables in the GISLine software (see, e.g., Revhaug 1999; Skogseth and Holsen 2010). To satisfy the Norwegian standard, all Norwegian software makes the adjustment in the map projection. The baselines' covariance matrices were also converted and scaled by a factor of one hundred. The chosen 3D-coordinate system for adjustments refers horizontally to the map projection EUREF89-UTM zone 32N. Vertically the reference is the ellipsoid. 3D parametric adjustments have been performed in two steps (see section 4).

3.5 Accuracy Analysis

In order to draw conclusions about the accuracy of the generated point clouds, all colored targets are positioned by GNSS. We then divide the ground control points into two categories. The points in one category are used in the georeferencing process of the images taken by UAV. The second category (check points) is used for the accuracy analysis. The coordinates of check points are determined in the images with Postflight Terra 3D software and then compared with GNSS-computed coordinates.

4. Sample aerial survey by eBee

A test area is selected on the grounds of NTNU and a sample aerial survey is carried out using eBee. Figure 3 shows the test area. The application area includes university buildings. The area covered by the eBee is 282 000 m^2. The image coordinate system is WGS84 and the ground control point coordinate system is EUREF89-UTM zone 32N, which provides output/results in the same coordinate system. Average ground sampling distance is 3.2 cm. 18 ground control points covering the selected area are chosen and positioned by applying RTK-GNSS surveys (see Figure 3). The GNSS receivers are Leica Viva CS15 controllers and GS15 antennas, shown in Figure 4 with a signalized color target. Two-step parametric adjustment is performed for positioning of 18 ground control points. A first order network of seven stations (called first order in this study) (see Figure 5) is established and then adjusted, based on classic static GNSS baselines of minimum one hour observation time. Three stations (Trondheim, NEW1 and NEW2) established in the test area, and four National Network Stations (Landsnettpunkter) (G24T0151, G24T0470, G24T0162 and G24T0477) established by Norwegian Mapping Authority, are used in the first order network. The four national network stations are fixed under the network adjustment and the coordinates of the three established stations in the test area are estimated. A full network analysis is then performed. No gross errors or problems with the fixed points were found. Results from the first order adjustment are shown in Table 1.

Table 1. The statistics of the first order network adjustment. The coordinates are in the EUREF89-UTM32N zone. Sd stands for the standard deviation. The unit of measurement is meters.

Check points computed by GNSS						
Point ID	**North (N)**	**East (E)**	**Ellipsoidal Height (H)**	**Sd N**	**Sd E**	**Sd H**
NEW1	7032492.1933	570484.2394	85.8330	0.001	0.001	0.003
NEW2	7032518.1182	570306.0786	75.9306	0.002	0.001	0.003
Trondheim	7032646.3030	570144.8641	110.0699	0.002	0.002	0.003

In the next step we compute the coordinates of the 18 ground control stations. In this study, this is called the second order network adjustment. In this second step, GNSS baselines with minimum five minute observation times have been used. The three points

(Trondheim, NEW1 and NEW2) from the first order adjustment were kept fixed under the adjustment. The 18 ground control points, signalized color target points (P1-P18), were positioned in the second order network adjustment. These 18 points are then classified in two groups, eight ground control points being used to fit the photogrammetric model, and ten check points being used for the accuracy investigation. Under the second measurement campaign, three GNSS receivers were installed on the fixed points (Trondheim, NEW1 and NEW2). A fourth GNSS receiver was then used as a rover in order to get three simultaneously measured baselines for each of 18 ground control points (see Figure 6). Except from station P11 and the height component of station P8, all standard deviations from the second order adjustment are less than 2mm. The estimated standard deviations might be too optimistic because they will not reflect centering errors and other factors. However, all the tribraches were controlled before and after the campaigns, and found to be within one millimeter horizontally. We believe this second order network to be very uniform and homogenous. It has an optimal inner geometry and a high level of precision among the signalized color target points P1-P18. Thus, they can be used as «true coordinate values» in the test of drone accuracy in this study.

Prior to the aerial photography, an aerial flight plan is derived. The aerial survey should be carried out at an altitude of about 97.5 m with longitudinal overlap of 80%, while lateral overlap is approximately 70%. 8 on-site ground control points are used for georeferencing. The remaining 10 points are then used for the accuracy analysis.

After carrying out the aerial survey with eBee, 215 of 217 captured images are used for further processing. Approximately 500000 3D tie points are identified and used. Due to the large number of images, the automatic generation of the 3D point cloud takes about 7 hours. Figure 7 shows the top view of the image positions captured over the test area as well as the ground control points. As a result a point cloud with about 14.4 million 3D densified points was computed, which leads to an average density of about 123 points per m^3. Figure 8 shows the derived point clouds covering the test area. The computation of a georeferenced 2D orthomosaic, and a DSM is then carried out using 8 ground control points. Figures 9 and 10 show the orthomosaic and the corresponding calculated digital surface model.

The main goal of this study is the accuracy investigation of photomapping using UAVs. Therefore, in the next step, the absolute accuracy of the generated point clouds are tested (indirectly) at the remaining 10 check points. A 2D positional standard deviation of 3.2 cm and height standard deviation of 4.3 cm are calculated. The mean of differences for east, north and height components are estimated at 0.1 cm, 1.2 cm and 5.3 cm, respectively (see Table 2).

The characteristics of residuals for all 18 ground control points are presented in Figure 11. Deviations in 3D position are depicted as vectors for all points. Horizontally, after comparing the vectors in Figure 11 no clear pattern or characteristic emerges. The points placed beyond the area of interest have reasonable accuracy, but there are some points even inside the area of the interest with larger residuals. This leads to the conclusion that no general statements about accuracy can be made. Vertically, measured height values from the model seem to be systematically larger than the «true values» from GNSS. Random variation was expected, but in this study we have too few check points to draw any conclusion.

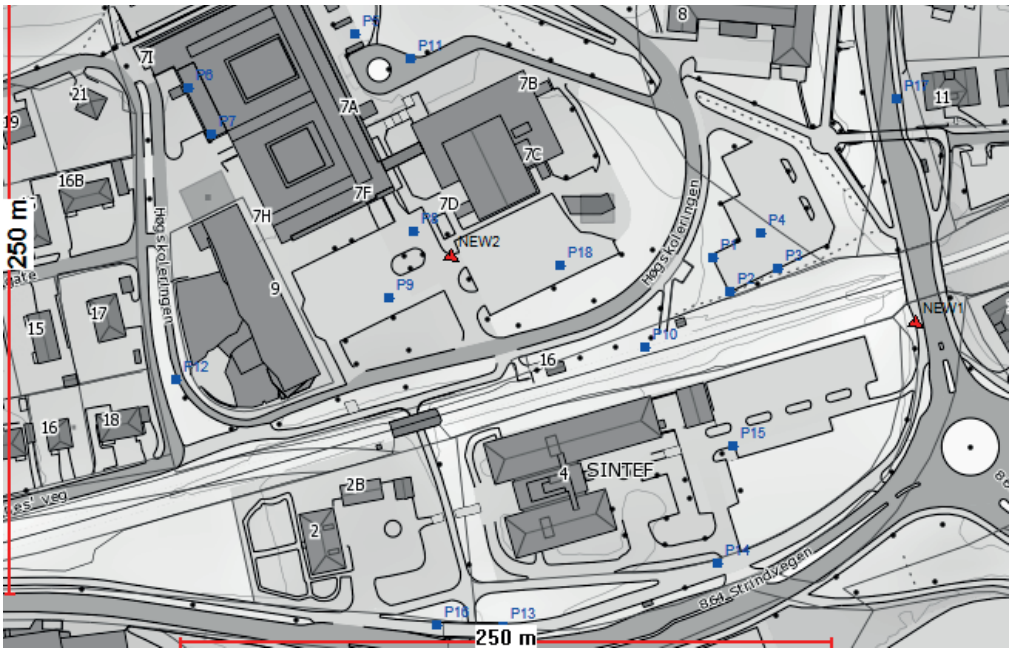

Figure 3. The test area at the Norwegian University of Science and Technology (NTNU).

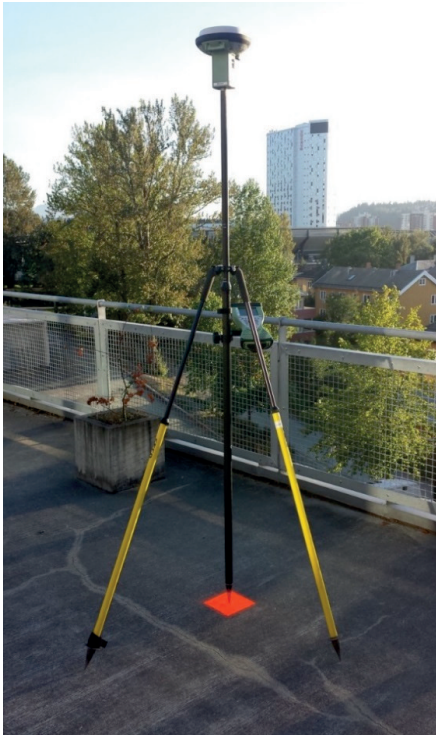

Figure 4. The GNSS receiver/antenna and the signalized color target

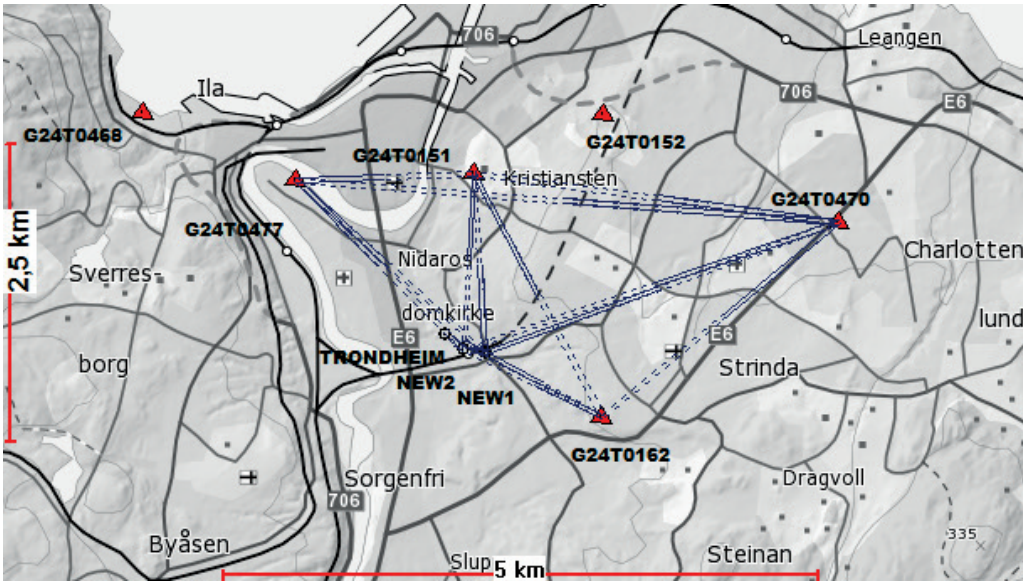

Figure 5. The first order network

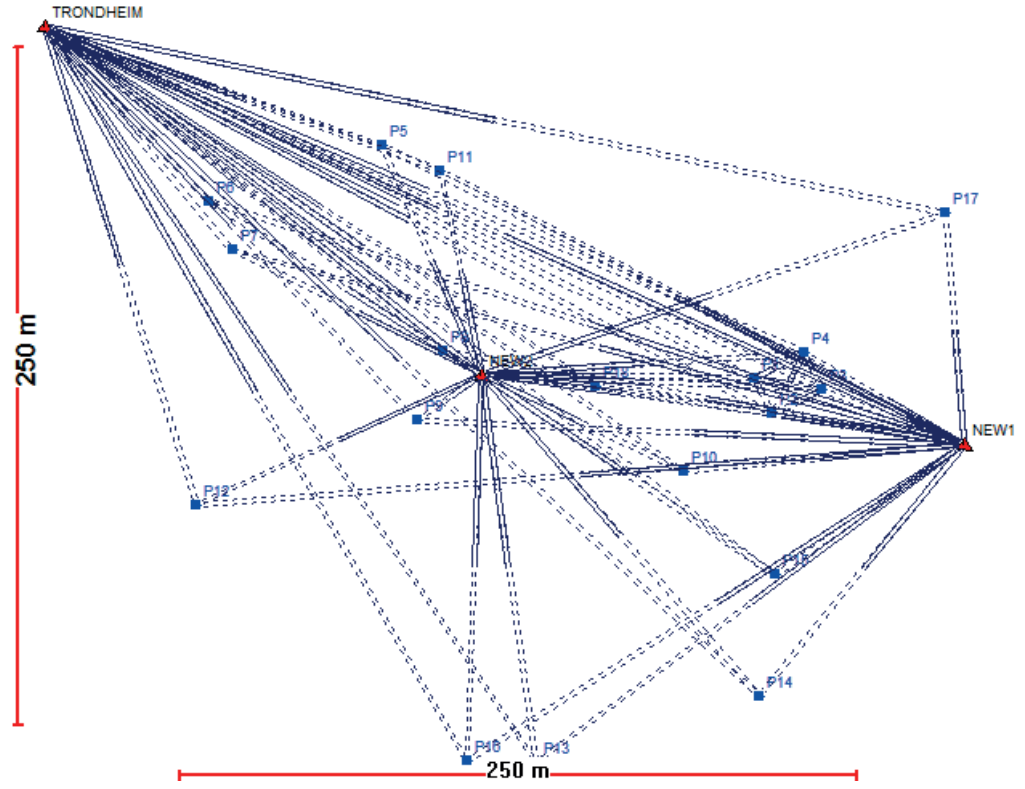

Figure 6. The second order network

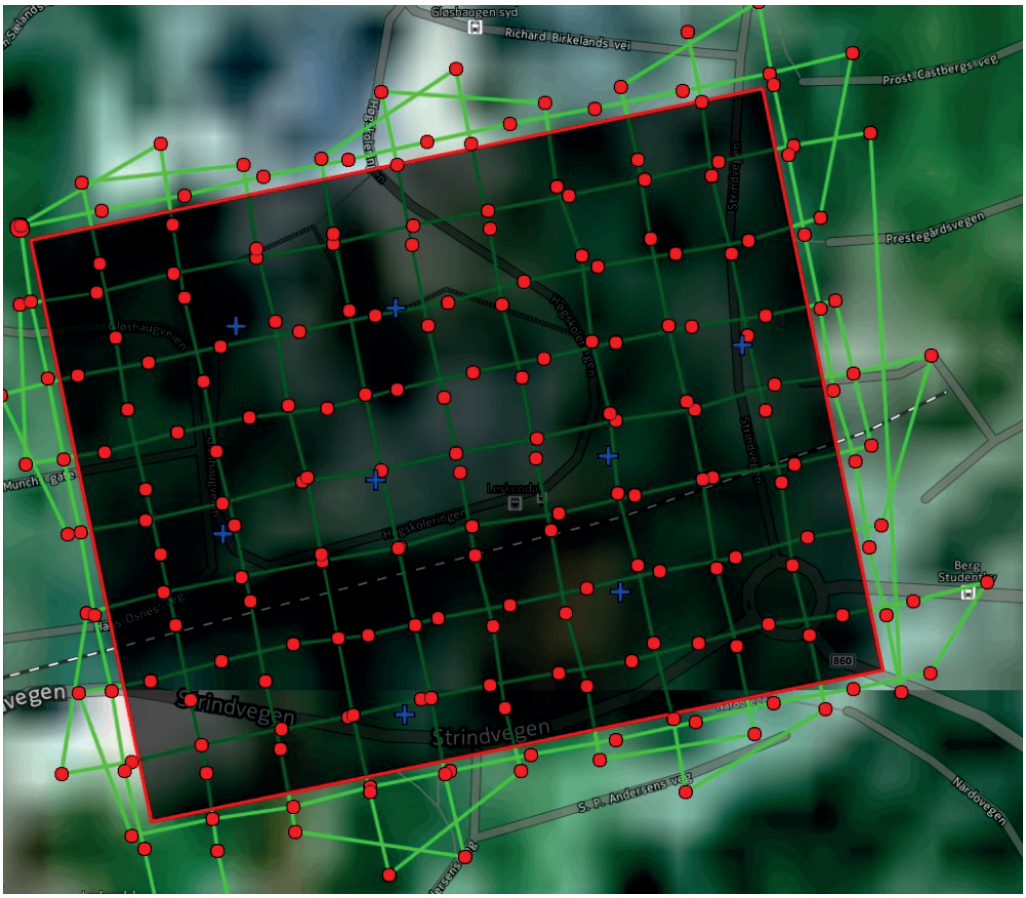

Figure 7. Top view of the captured image positions (red dots) and ground control points (blue crosses) over the test area. The green line follows the position of the image in time starting from the large red dot in top-left corner of the test area.

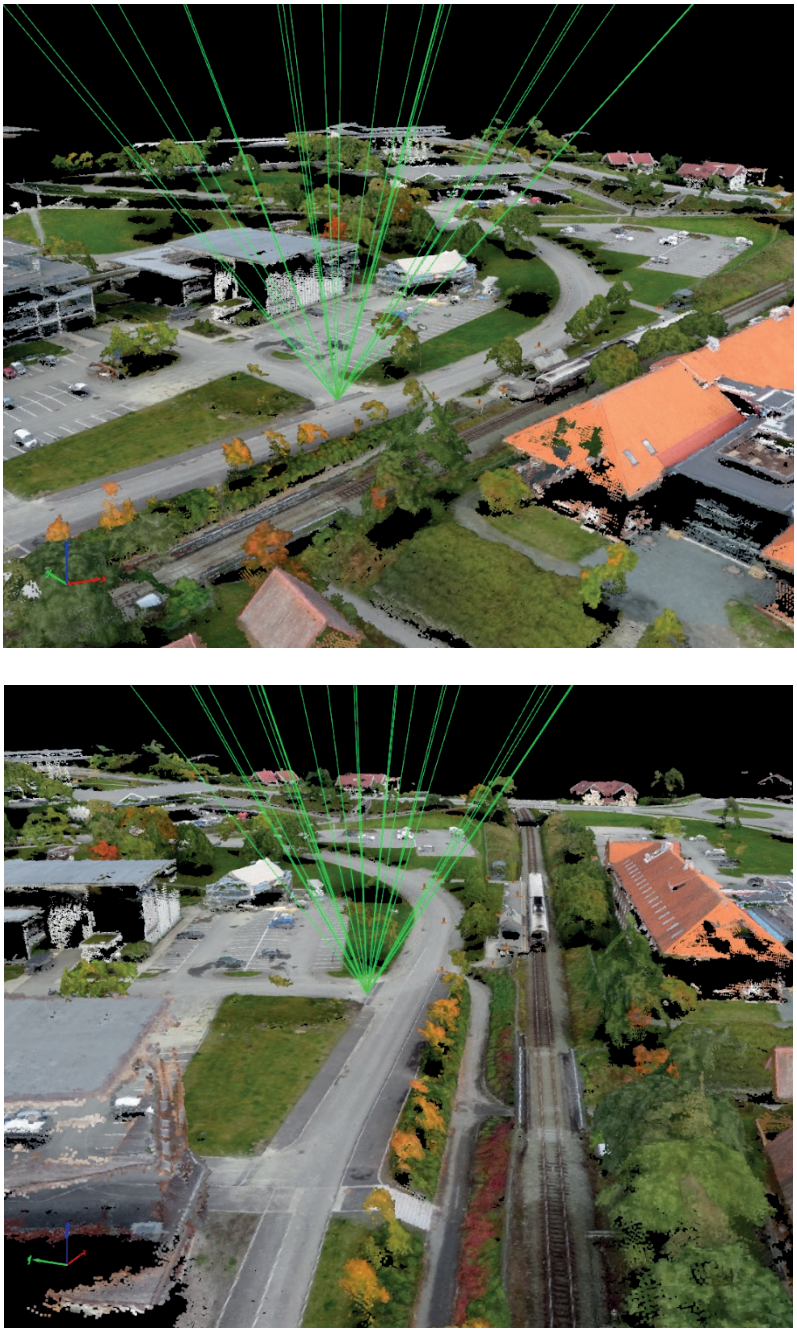

Figure 8. Point cloud generated with Postflight Terra 3D from two points of view.

Figure 9. The orthomosaic of the test area generated with the Postflight Terra 3D (professional photogrammetry).

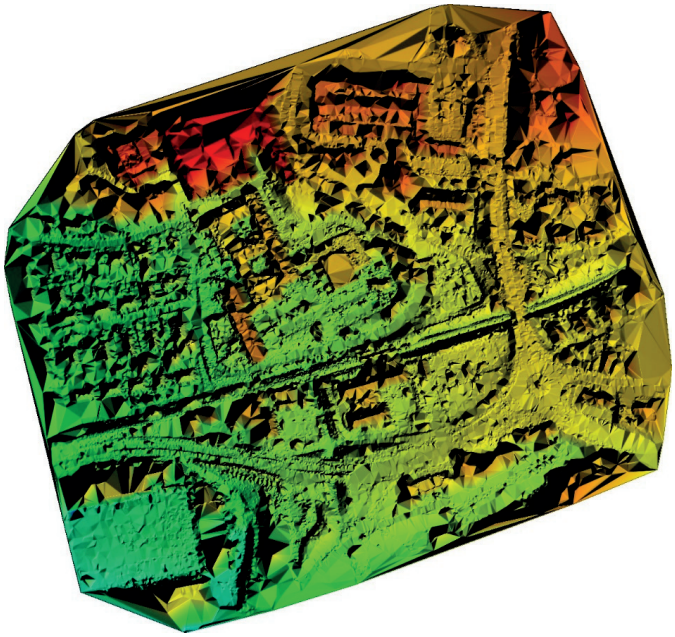

Figure 10. The Digital Surface Model of the test area generated with the Postflight Terra 3D (professional photogrammetry)

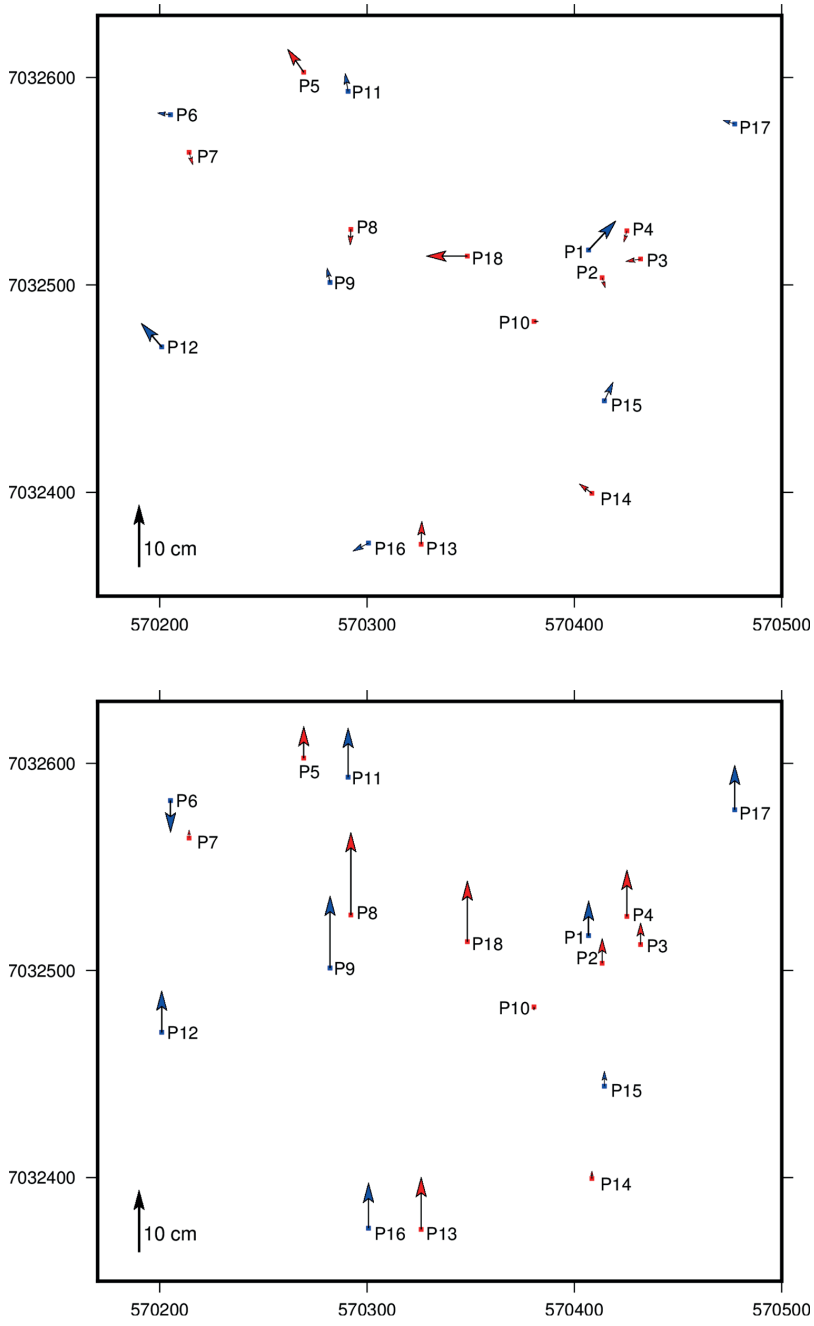

Figure 11. Deviations of the point cloud and the GNSS-computed ground control points. The 2D horizontal deviations (top) and the height deviations (bottom). Blue: points used in the georeferencing. Red: Control points not used in the georeferencing.

Table 2. The statistics of the check points computed by GNSS (top) and check points measured in the images with Postflight Terra 3D (middle); deviations between the two sets of coordinates (bottom). The coordinates are in the EUREF89-UTM32N zone. Sd stands for the standard deviation. The unit of measurement is meters.

Check points computed by GNSS						
Point ID	**North (N)**	**East (E)**	**Ellipsoidal Height (H)**	**Sd N**	**Sd E**	**Sd H**
P2	7032503.4822	570413.3669	80.1282	0.001	0.001	0.001
P3	7032512.5002	570431.9676	80.4122	0.001	0.001	0.001
P4	7032526.0900	570425.3519	80.6571	0.001	0.001	0.001
P5	7032602.5627	570269.4359	79.5778	0.001	0.001	0.002
P7	7032563.9401	570214.1377	83.7857	0.001	0.001	0.002
P8	7032526.8019	570292.1450	75.8363	0.002	0.001	0.003
P10	7032482.3970	570380.5116	78.9091	0.001	0.001	0.002
P13	7032374.9648	570326.0843	78.1933	0.001	0.001	0.002
P14	7032399.5143	570408.4605	81.1564	0.001	0.001	0.002
P18	7032513.9047	570348.3729	75.7412	0.001	0.001	0.002

Check points measured in the images with Postflight Terra 3D			
Point ID	**North (N)**	**East (E)**	**Ellipsoidal Height (H)**
P2	7032503.466	570413.372	80.168
P3	7032512.496	570431.944	80.447
P4	7032526.072	570425.347	80.732
P5	7032602.600	570269.410	79.629
P7	7032563.920	570214.144	83.799
P8	7032526.777	570292.144	75.969
P10	7032482.397	570380.519	78.904
P13	7032375.002	570326.085	78.277
P14	7032399.529	570408.441	81.168
P18	7032513.905	570348.307	75.839

Deviations in check points between Postflight Terra 3D and GNSS			
Point ID	**Deviations (N)**	**Deviations (E)**	**Deviations(H)**
P2	–0.016	0.005	0.040
P3	–0.004	–0.024	0.035
P4	–0.018	–0.005	0.075
P5	0.037	–0.026	0.051
P7	–0.020	0.006	0.013
P8	–0.025	–0.001	0.133
P10	0.000	0.007	–0.005
P13	0.037	0.001	0.084
P14	0.015	–0.020	0.012
P18	0.000	–0.066	0.098
Mean	0.001	–0.012	0.053
Sd	0.023	0.023	0.043
Sd 2D	0.032		

5. Conclusion

A workflow is presented for generation of 3D point clouds from digital imagery captured by a low-cost UAV, eBee. In investigation of the absolute accuracy of a georeferenced 3D point cloud, deviations are found to be small even though a low-cost UAV is used. An absolute two-dimensional standard deviation of 3.2 cm means that UAV photogrammetry is applicable for topographic surveys. A successful application using the example of a university campus survey is presented. In light of the high operational cost of classical aerial photogrammetry, UAV photogrammetry offers a way to take advantage of extensive data acquisition quickly and at low cost.

References

Ahmad, A. (2011). Digital mapping using low altitude UAV. *Pertanika Journal of Science and Technology* 19: 51–58.

Eisenbeiß, H. (2009). UAV photogrammetry. Dissertation, Institut für Geodäsie und Photogrammetrie an der ETH Zürich, Mitteilungen Nr. 105.

Harwin, S. and A. Lucieer (2012). Assessing the accuracy of georeferenced point clouds produced via multi-view stereopsis from unmanned aerial vehicle (UAV) imagery. *Remote Sensing* 4: 1573–1599.

Kraus, K. (2011). *Photogrammetry- Geometry from images and laser scans.* De Gruyter.

Mancini, F., M. Dubbini, et al. (2013). Using unmanned aerial vehicles (UAV) for high-resolution reconstruction of topography: The Structure from Motion Approach on Coastal Environments. *Remote Sensing* 5: 6880–6898.

Mills, JP. and I. Newton (1996). A new approach to the verification and revision of large scale mapping. *ISPRS Journal of Photogrammetry & Remote Sensing* 51: 17–27.

Mills, JP., I. Newton, et al. (1996). Aerial photography for survey purposes with a high resolution, small format, digital camera. *Photogrammetric Record* 15 (88): 575–587.

Revhaug I. (1999). A model for the transformation of satellite vectors to the plane of the map. *Survey Review* 35 (274): 277–285. doi:10.1179/003962699791483680

Rosnell, T. and E. Honkavaara (2012). Point cloud generation from aerial image data acquired by a quadrocopter type micro unmanned aerial vehicle and a digital still camera. *Sensors* 12: 453–480.

Skogseth, T. and J. Holsen (2010). *Basic GPS*. NTNU Compendium. Division of Geomatics.